Dalton Transactions

Accepted Manuscript

ROYAL SOCIETY OF CHEMISTRY

www.rsc.org/dalton

Controllable synthesis of Zn/Cd(II) coordination polymers: dual-emissive luminescent properties, and tailoring emission tendency under varying excitation energy

Kai Xing,[a] Ruiqing Fan,*[a] Song Gao,[a] Xinming Wang,[a] Xi Du,[a] Ping Wang,[a] Ru Fang,*[b] and Yulin Yang*[a]

[a] Department of Chemistry, Harbin Institute of Technology, Harbin 150001, P. R. China

[b] Department of Mathematics, Harbin Institute of Technology, Harbin 150001, P. R. China.

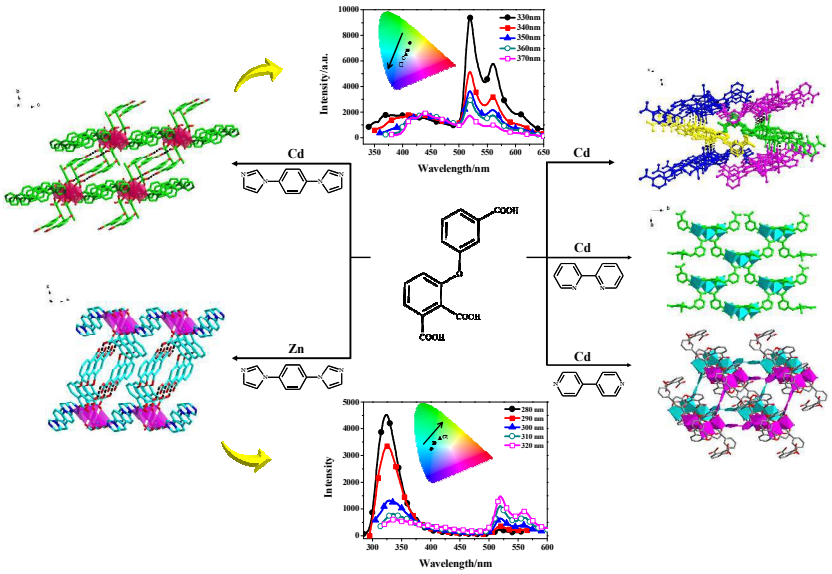

Under the help of rationally selected N-donor ligands, different dimensional architectures **1-5** have been synthesized and they display dual-emission property.

Controllable synthesis of Zn/Cd(II) coordination polymers: dual-emissive luminescent properties, and tailoring emission tendency under varying excitation energy

Kai Xing,[a] Ruiqing Fan,[*a] Song Gao,[a] Xinming Wang,[a] Xi Du,[a] Ping Wang,[a] Ru Fang,[*b] and Yulin Yang[*a]

[a] Department of Chemistry, Harbin Institute of Technology, Harbin 150001, P. R. China

[b] Department of Mathematics, Harbin Institute of Technology, Harbin 150001, P. R. China.

To whom the proofs and correspondence should be sent.

Professor Rui-Qing Fan

Department of Chemistry

Harbin Institute of Technology Harbin 150001, P. R. China

Fax: +86-451-86413710

E-mail: fanruiqing@hit.edu.cn, ylyang@hit.edu.cn and fangr@hit.edu.cn

Abstract

Based on a new asymmetric semi-rigid V-shape tricarboxylate ligand 3-(2′,3′-dicarboxylphenoxy)benzonic acid (H_3dpob), a series of zinc/cadmium(II) coordination polymers, $\{[Cd(Hdpob)(H_2O)_3]\cdot H_2O\}_n$ (**1**), $[Cd(Hdpob)(bib)]_n$ (**2**), $[Zn(Hdpob)(bib)_{0.5}]_n$ (**3**), $\{[Cd_{1.5}(dpob)(2,2'\text{-bipy})]\cdot 0.5H_2O\}_{2n}$ (**4**) and $\{[Cd_3(dpob)_2(4,4'\text{-bipy})_2]\cdot 3H_2O\}_n$ (**5**) [bib = 1,4-bis(1-imidazoly)benzene; 2,2′-bipy = 2,2′-bipydine; 4,4′-bipy = 4,4′-bipydine], have been successfully synthesized *via* hydro(solvo)thermal reactions. **1** forms a three dimensional (3D) supramolecular structure linked by two types of intermolecular hydrogen bonds based on zig-zag 1D chains. Whereas **2** and **3** are obtained similar 2D layer structure by same ligands and further connected into 3D structure through hydrogen bonds. **4** displays a homochiral 2D structure though two achiral ligands 2,2′-bipy and H_3dpob, which contains right-hand helical infinite chains. **5** is a 3D structure containing 2D metal-pyridine layers motifs, which are further pillared by beaded $dpob^{3-}$ ligands to complete the structure and form a 6-connected **pcu** (primitive cubic) net. In DMSO solvent, **1-5** all illustrate dual-emission properties but have different low-energy emission (LE) intensity relatively. Extraordinarily, the difference generating from central metals between **2** and **3** makes the intensity of LE dramatically enhanced and quenched. In this regard, the luminescence of **2** and **3** can be tuned between blue and green regions by varying the excitation light, and tuning tendency can be tailored with inverse directions. Comparing their tunable-sensitivity to energy quantitatively, the theoretical calculation displays that **3** (4.29%) is little higher than **2** (3.59%) in relative lower excitation wavelength zone. Meanwhile, five coordination polymers show distinct luminescence thermochromism in the solid state. When temperature decreases from 298 K to 77 K, red-shift from blue/green to pure yellow light is highlighted. The fantastic and unique luminescence phenomenon not only brings an insight into synthesis of dual-emissive materials, but helps us to understand luminescence behavior deeply as well.

Introduction

Dual-emissive luminescent materials have been under intensive investigation as chemical biosensors and luminescent probes since their distinct optical signals resulting from their interesting environment-responsive properties.[1-3] Design concept of tunable dual-emissive luminescent material has enabled real-time and in vivo tumor hypoxia imaging with excellent temporal and spatial resolutions.[4, 5] The strategy constructing dual-emissive material, in the previous studies, generally and normally focus on the method of linking two chromophores within a supramolecular assembly,[6, 7] since it becomes easy to control the emission by exciting different luminophores with different excitation energies.[8] Nevertheless, the low thermal stability of these materials based on organic molecules limits their applications.[9, 10] Notably, metal-organic coordination polymers as hybrid materials consisted of organic ligands and inorganic metal ions constituents may overcome the issue and raise satisfaction to require at same time.[11, 12] Hence, it is taken as a new platform to explore dual-emissive luminescence materials with tunable colors emission. Undoubtedly, the judicious selection of ligands plays a crucial role in the construction of novel coordination polymers owing to their abundant coordination modes to satisfy the geometric requirement of metal centers in constructing fascinating structural architectures. To date much of the work has been focused mainly on symmetrical carboxylate ligands and little attention has been paid to asymmetric multicarboxylate ligands.[13-15] One of our research lines is devoted to study the interaction of the asymmetric semi-rigid V-shape tricarboxylate ligand and the different N-donor ligand to construct diverse architectures. Among them, Zn/Cd(II) transition metal-organic coordination polymers have attracted many researchers' attention for their lower-cost and highly luminescent efficiency.[16-19]

Moreover, the luminescent properties of some metal-organic coordination polymers are highly sensitive to the surrounding environment.[20] In this context, tuning behaviors of dual-emissive coordination polymers responding to various cryogenic temperatures[21-24] and excitation energy[25-28] is a vast and rich field containing a certain number of literature entries. In contrast, the properties referring to solvent molecules related or induced interaction have been investigated to a much lesser extent. To the best of our knowledge, the direct contribution to luminescence cannot belong to metal center, however, the disturbance should not be absolutely neglected. Particularly, to

the elements in the same main or subgroup, the tiny distinction like electron arrangement or ionic radium may give rise to some amazing result beyond expectation in whole tuning emission process.[29-31] Our research will be carried out along the pathway of solving the shortage and the detail mentioned above.

In this work, we have been successfully isolated a series of Zn/Cd(II) metal coordination polymers *via* a new semirigid V-shaped asymmetric tricarboxylate ligand. The main ligand we chose has never been reported in previous literature and also coordinates with Zn/Cd(II) transition metal firstly. The similar reported ligands are summarized in Table S1. As start, **1** is built by single H_3dpob, which shows 1D chain on account of obstacle of coordinated water molecules. For further improving dimension, we construct **2-5** based on the strategy of inducing different N-donor ligands by changing the structural parameter of themselves such as length and coordinated position, thus obtain three different 2D layers for **2-4** and 3D structure for **5** respectively. **1-5** all display dual-emission properties in DMSO. It is worth noted that although **2** and **3** own same ligands and similar structure, they exhibit dual-emission tunable luminescence with inverse tendency ranging from blue and green based on the variation of excitation light in DMSO. Meanwhile, **3** shows superiority than **2** in the tunable-sensitivity to excitation energy. It might bring up a novel and strategic synthesis tip, for realizing both color and tendency tunes of dual-emission coordination polymers *via* varying the wavelength of excitation and gain a chance to clarify how metal ions influence the coordination environment, the configuration of ligands, fluorescence features and tunable-sensitivity to energy by degrees.

Results and discussion

Synthesis

We have successfully obtained five new Zn/Cd(II) coordination polymers from one-dimensional chain to three-dimensional network and the reaction routes of **1**–**5** are shown in Scheme 1. 1D structure of **1** is prepared by single semirigid V-shaped tricarboxylate ligand H_3dpob. Owing to the fact that the coordinated water molecules prevent the linkage between the neighboring chains, we decide to introduce N-donor rigid auxiliary ligand to compete with coordinated water molecules. For N-donor rigid ligand, generally, important factors determining final structure mainly focus on the positions of coordinating points and shape of ligand itself. Firstly, it is appropriate to

choose easily chelating 2,2′-bipy ligand. As show in **4**, 2D layer structure are observed, which effectively avoids the coordination of water molecules with raising the dimension of structure from 1D (**1**) to 2D (**4**), and that proves the strategy we mentioned before is feasible. Furthermore, we only change the position of N atoms in auxiliary ligand, and adopt the 4,4′-bipy with terminal coordinate sites as replacement. To some extent, this terminal configuration makes 4,4′-bipy itself as a "connecting pillar" in the frame structure. Hence, 3D structure of **5** is obtained. Thirdly, 4,4′-bipy is replaced by bib as auxiliary ligand, comparatively, the position of N atoms is similar but the length of ligand increases from 7.06 **Å** to 9.86 **Å**. As we expected, new structures appear in **2** and **3**, which are different from **5**. The tiny differences enbodying in structure between **2** and **3** may be caused by metal ions. Comparison of Zn(II) to Cd(II), although they both have d^{10} full-filled electron orbit in the same subgroup, their ionic radium are distinct different, which may lead to diversity in bond strength, bond lengths and bond angles even with the same organic ligands forming the covalent bonds. In a word, the enriched structures of **1**-**5** are realized by changing N-donor auxiliary ligands. These little differences of structure may actually make huge impact in specific properties beyond our knowledge before.

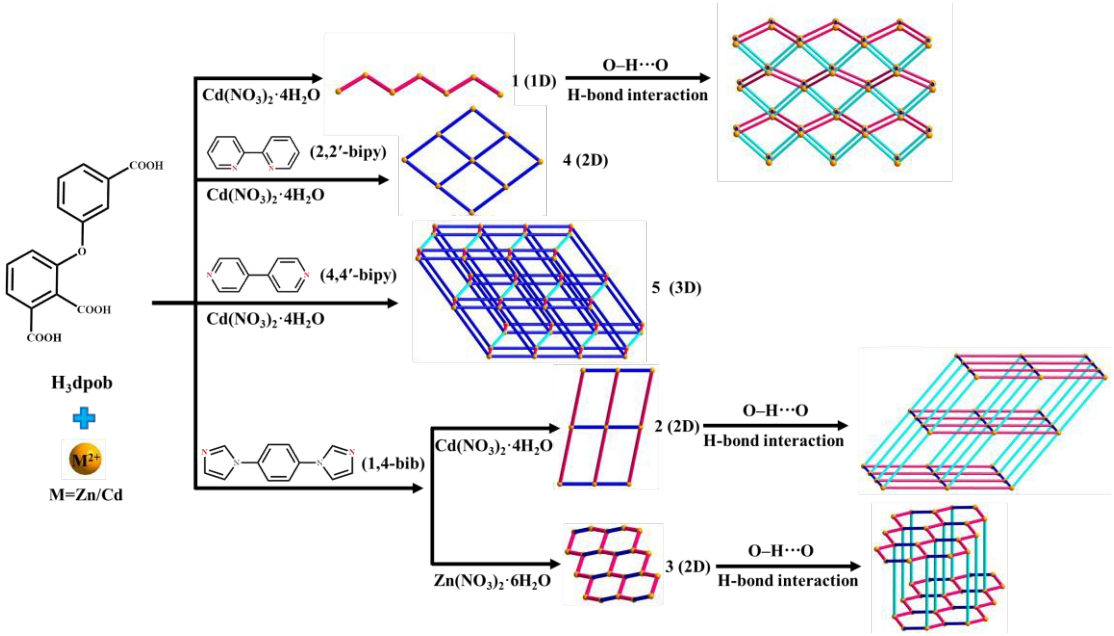

Scheme 1 Reaction routes of coordination polymers **1–5.**

Table 1. Crystal data and structure refinement parameters of coordination polymers **1**–**5.**

Identification code	1	2	3	4	5
Empirical formula	$C_{15}H_{16}O_{11}Cd$	$C_{27}H_{18}N_4O_7Cd$	$C_{21}H_{13}N_2O_7Zn$	$C_{50}H_{31}N_4O_{15}Cd_3$	$C_{50}H_{36}N_4O_{17}Cd_3$
Formula mass	484.68	622.86	470.72	1264.99	1302.03
Crystal system	Orthorhombic	Triclinic	Triclinic	Orthorhombic	Triclinic
Space group	*P*bca	$P\bar{1}$	$P\bar{1}$	*C*222(1)	$P\bar{1}$
a (Å)	12.703	7.8553(11)	6.9785(16)	13.7884(7)	13.862(3)
b (Å)	9.444	11.9933(17)	9.550(3)	18.0779(7)	14.477(3)
c (Å)	29.401	13.9255(19)	14.549(4)	17.6422(8)	14.664(4)
α (˚)	90	109.566(2)	108.260(8)	90	95.331(7)
β (˚)	90	99.334(3)	95.880(8)	90	106.021(7)
γ (˚)	90	94.642(3)	92.854(8)	90	118.084(6)
V (Å^3)	3527.0	1206.8(3)	912.5(4)	4397.6(3)	2407.7(10)
Z	8	2	2	4	2
D_c/(g · cm^{-3})	1.825	1.714	1.713	1.911	1.796
μ (Mo Kα)/mm^{-1}	1.297	0.962	1.398	1.519	1.393
F(000)	1936	624	478	2492	1288
θ range (˚)	2.12 –27.53	1.82 – 27.49	3.07 – 26.35	3.17 – 26.39	3.00 – 25.50
Limiting indices	$-15 \le h \le 16$ $-12 \le k \le 12$ $-28 \le l \le 38$	$-8 \le h \le 10$ $-15 \le k \le 15$ $-17 \le l \le 18$	$-7 \le h \le 8$ $-11 \le k \le 11$ $-15 \le l \le 18$	$-17 \le h \le 17$ $-17 \le k \le 22$ $-22 \le l \le 20$	$-16 \le h \le 16$ $-17 \le k \le 17$ $-16 \le l \le 17$
Data/Restraints/Parameters	4006 / 1 / 244	5298 / 0 / 352	3524 / 0 / 280	4394 / 0 / 326	8699 / 0 / 667
GOF on F^2	0.882	0.825	0.806	1.059	0.853
Final *R* indices [$I > 2\sigma(I)$]					
R_1[a]	0.0371	0.0475	0.0466	0.0272	0.0547
wR_2[b]	0.1090	0.1188	0.1084	0.0423	0.1279
R indices (alldata)					
R_1	0.0614	0.0705	0.0986	0.0371	0.1335
wR_2	0.1318	0.1389	0.1395	0.0444	0.1676
CCDC	1401569	1401570	1401571	1401572	1401573

[a] $R_1 = \sum||F_o| - |F_c|| / \sum|F_o|$; [b] $wR_2 = [\sum[\, w\,(F_o^2 - F_c^2)^2] / \sum[\, w\,(F_o^2)^2]]^{1/2}$.

Description of crystal structure

{[Cd(Hdpob)(H_2O)$_3$]·H_2O}$_n$ (1) Single-crystal X-ray diffraction analysis of coordination polymer **1** crystallizes in the orthorhombic space group of *P*bca, and its asymmetric unit contains one Cd(II) ion, one partly deprotonated $Hdpob^{2-}$ ligand, three coordinated water molecules and one free water molecule. As shown in Fig. S1, the metal center Cd1 is seven-coordinated by four oxygen atoms from the two individual $Hdpob^{2-}$ ligands (O4, O5, O6 and O7) and three oxygen atoms from the coordinated water molecules (O8, O9 and O10), forming a slightly distorted single-capped octahedron (Fig. 1a). The distance between two Cd^{2+} ions is 5.643(5) Å, each $Hdpob^{2-}$ ligand links two Cd(II) ions with its two carboxyl groups both adopting a bidentate-chelating coordination fashion, and bond lengths of Cd–O vary from 2.288(3) to 2.641(3) Å, respectively. All Cd–O bond lengths are in the range expected for such coordination polymers.[32-34] In the 3-carboxylic group of ligand, the bond lengths of C–O of deprotonated carboxyl groups vary from 1.234(3) to 1.269(3) Å. However, the length of C4–O2 bond is 1.317(2) Å, which is longer than that of C4–O1. According to difference lengths of C–O bond, 3-carboxylic group (O1-C4-O2) is non-deprotonated. Two adjacent Cd(II) ions are connected through O1, O2, O3 and O4 atoms deriving from two different $Hdpob^{2-}$ ligands, giving rise to a zig-zag 1D chain (Fig. 1b). The coordinated water molecules prevent the linkage between the neighboring chains into a higher dimensional structure. Luckily, two types of intermolecular hydrogen bonds make the 1D chains into a 3D supramolecular framework. One is between uncoordinated carboxyl groups and carboxyl groups belonging to another $Hdpob^{2-}$ ligand (O2–H2⋯O5 = 1.798 Å), giving a 2D wave-like layer in *bc* plane (Fig. 1c). The other is under helping of $Hdpob^{2-}$ ligand and coordinated water molecule (O8–H8⋯O4 = 2.238 Å), thus these 2D layers are connected into a 3D supramolecular structure (Fig. 1d). Topological analysis has been applied for better understanding the connectivity of 3D framework in **1**. When we consider the Cd(II) cation as a 6-connected octahedral node, the $Hdpob^{2-}$ ligand and hydrogen bond interactions as the linkers, the simplified topological representation of **1** can be described in Fig. 1e, which exhibits a 3D 6-connected **pcu** (primitive cubic) topological type with point symbol ($4^{12}.6^3$).

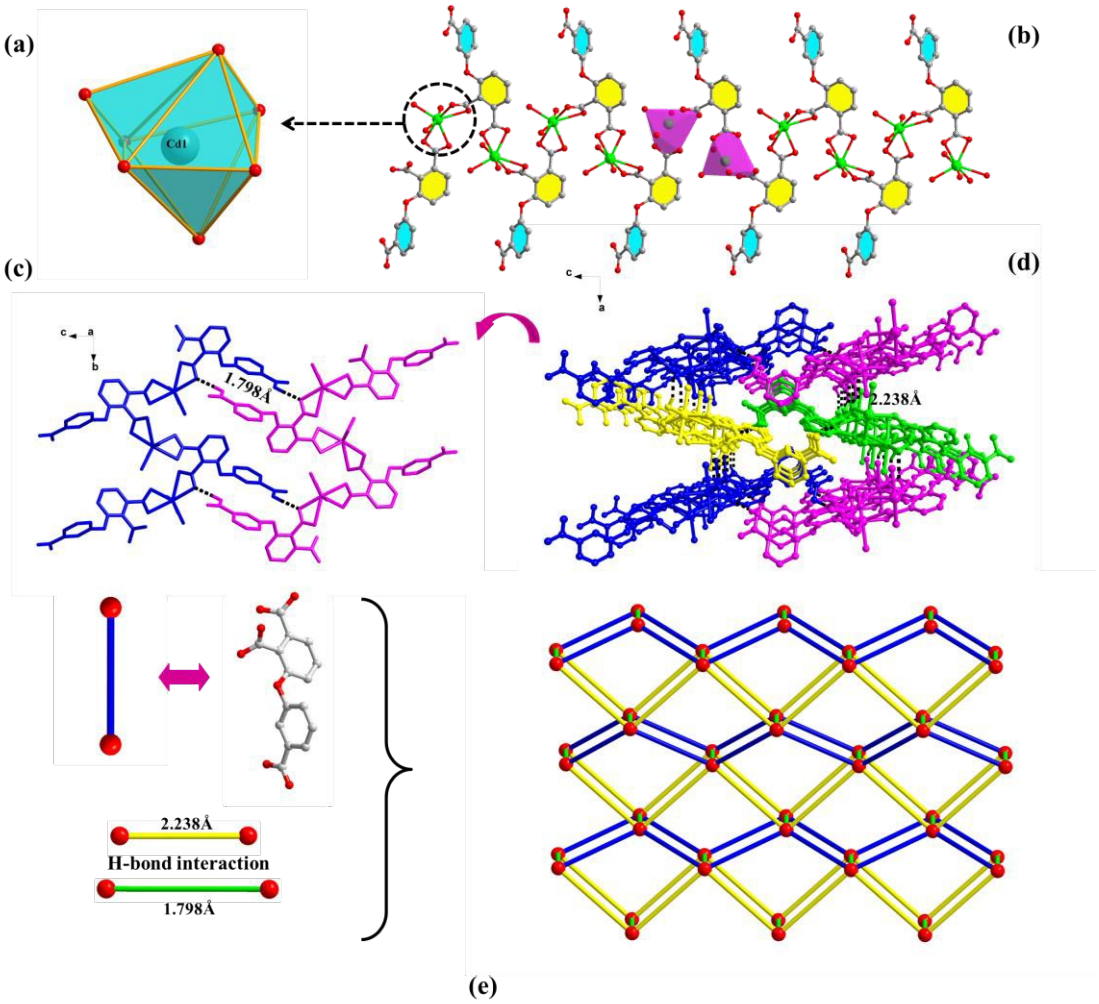

Fig. 1 (a) Polyhedral representation of the coordination sphere of the Cd centre in **1**. (b) Polyhedral and ball–and–stick representation of the 1D "wave-like" chain structure along *b* axis in **1**. (c) Stick representation of the 2D layer in **1**. (d) A 3D supramolecular structure of **1** (hydrogen bonds are shown by black dash line). (e) The 3D **pcu** topology in its most symmetrical form distinguished by different colors (color code: Cd(II) cation, red ball).

[Cd(Hdpob)(bib)]$_n$ (2) Coordination polymer **2** was synthesized by introducing rod-like N-donor (bib) secondary ligand. X-ray diffraction analysis shows that the asymmetric unit consists of one crystallographically independent Cd^{2+} cation, one $Hdpob^{2-}$ ligand and one bib ligand (Fig. S2). Metal center Cd1 is six-coordinated by four oxygen atoms (O1, O1A, O2A and O3A) from three $Hdpob^{2-}$ ligands, two nitrogen atoms N1 and N3 from two bib ligand molecules, displaying distorted octahedron geometry arrangement with [CdO_4N_2] coordination environment (Fig. 2a). Owing to the existence of oxygen bridges (O1 and O1A), two adjacent octahedrons sharing a common side form a binuclear cluster, and the other two oxygen atoms

deriving from each $Hdpob^{2-}$ ligand adopt a bidentate coordination mode μ_2-η_O^1:η_O^1 to connect adjacent binuclear clusters (Scheme 2b). The lengths of Cd–O bond range from 2.269(4) to 2.497(3) Å. Nitrogen atoms from two imidazole rings display the η_N^1 mode to connect metal center Cd1 with Cd–N bond lengths of 2.287(4) and 2.247(4) Å and the N–Cd–N bond angle is 173.8 (13)°. It was also found that the separations of Cd1···Cd1A are 3.709 and 4.337 Å.

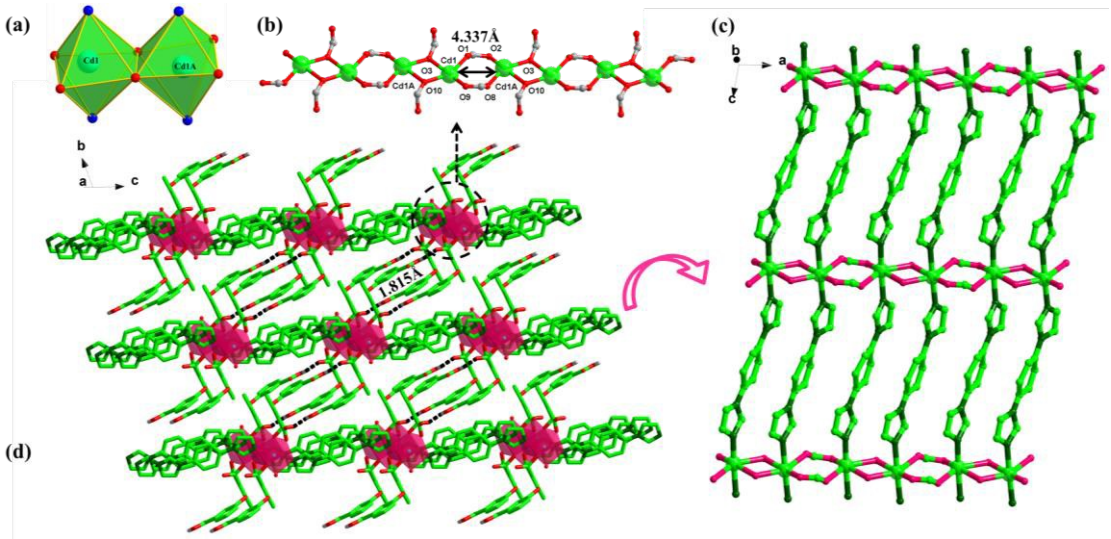

Fig. 2 (a) Polyhedral representation of the coordination sphere of the Cd1 and Cd1A centers in **2**. (b) It shows the infinite $[Cd–O/COO]_n$ chain along *a* axis in **2**. (c) The illustration of 2D layer of **2** in *ac* plane. (d) A 3D supramolecular structure of **2** (hydrogen bonds are shown by black dash line).

The neighboring Cd^{2+} are linked by partly deprotonated $Hdpob^{2-}$ ligands, forming 1D chains of [-Cd1-$(CO_2)_2$-Cd1A-O_2-] along *a* axis (Fig. 2b). Then the 1D chains are further connected *via* nitrogen atom of bib ligand and expanded in *ac* plane (Fig. 2c). The 2D layer is prevented from forming a higher order dimensional network by the terminal uncoordinated carboxyl groups that hang beside the two sides of the layer. In addition, the resulting layers are parallel to each other and connected into a 3D dense framework by rich O–H···O hydrogen bond interactions ($d_{H\cdots O}$ = 1.815 Å) (Fig. 2d), which can be simplified as 6-connected **pcu** topological type (Fig. 3).

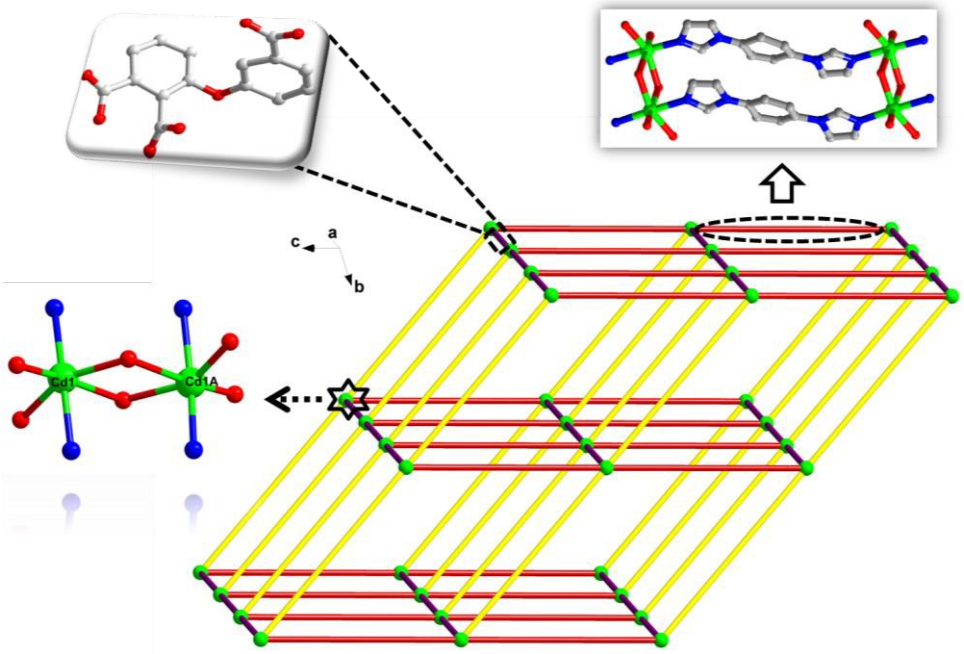

Fig. 3 Topological view of the 3D structure of **2** with the 6-connected **pcu** net (color code: the binuclear unit [CdO_4N_2], green ball; the defined linkers of bib and $Hdpob^{2-}$ ligand, red and purple sticks).

[Zn(Hdpob)(bib)$_{0.5}$]$_n$ (3) Coordination polymer **3** crystallizes in triclinic space group *P*-1. Different from the case for **2**, there is only half crystallographically independent bib in the asymmetric unit in **3**. As shown in Fig. S3, the Zn(II) center presents a tetrahedral coordination geometry (Fig. 4a), which is coordinated by three carboxyl oxygen atoms (O1, O3 and O4) from distinct $Hdpob^{2-}$ ligands and a nitrogen atom from bib ligand. In **3**, bib ligand displays η_N^1 mode to connect Zn(II) as well, with Zn–N bond length of 1.977(3) Å, and $Hdpob^{2-}$ ligands adopt bidentate-monatomic bridge μ_3-η_O^1:η_O^2 coordination fashion to connect three Zn^{2+} ions, The distance of the Zn–O bond ranges from 1.916(3) to 1.963(3) Å and the O–Zn–O bond angle is from 101.4**(**14) to 122.8(14)°.

Along *a* axis, partly deprotonated $Hdpob^{2-}$ ligands connect Zn^{2+} into a 1D chain (Fig. 4b), and bib ligands combine two chains and construct a distorted layer in *ab* plane (Fig. 4c), that make **3** displays a wavelike chain in *b* direction. Between the neighboring layers the obvious hydrogen bonds are observed, the distance of O7–H7···O4 is 1.860 Å, and leads to a 3D supramolecular framework (Fig. 5a). After topological analysis to **3,** the whole structure shows the 5-connected **bnn** (boron nitride) type network with the Schläfli symbol $\{4^6 \cdot 6^4\}$ (Fig. 5b).

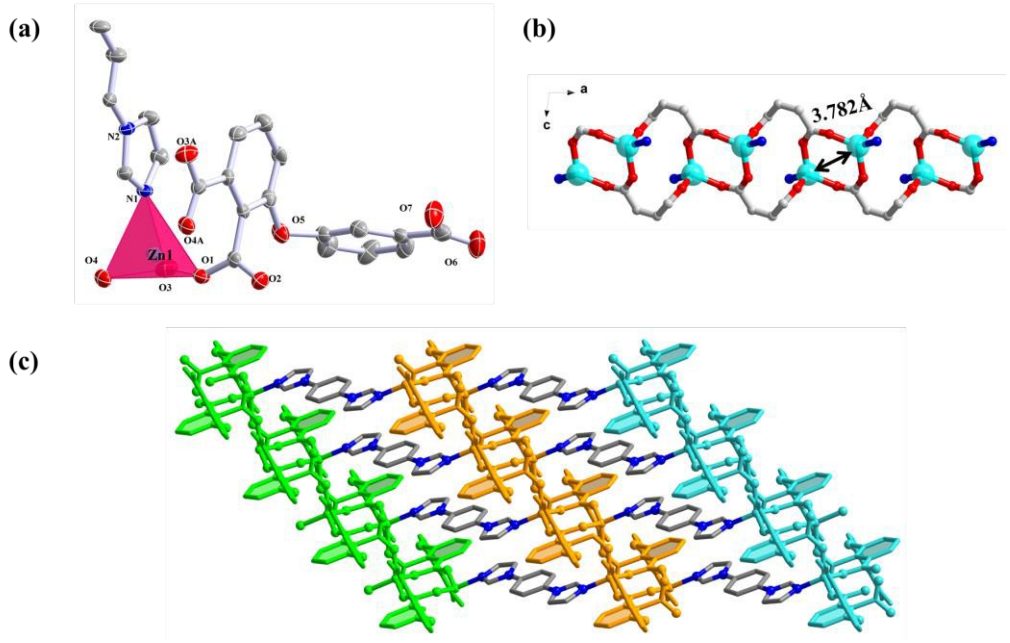

Fig. 4 (a) The structural unit of **3** with labeling scheme and 50% thermal ellipsoids (hydrogen atoms are omitted for clarity). Symmetry codes: O3A *1+x, y, -z*; O4A 1-*x, 1-y, 1-z*. (b) It shows the infinite $[Zn–O/COO]_n$ chain along *a* axis in **3**. (c) The illustration of 2D layer of **3** in *ab* plane.

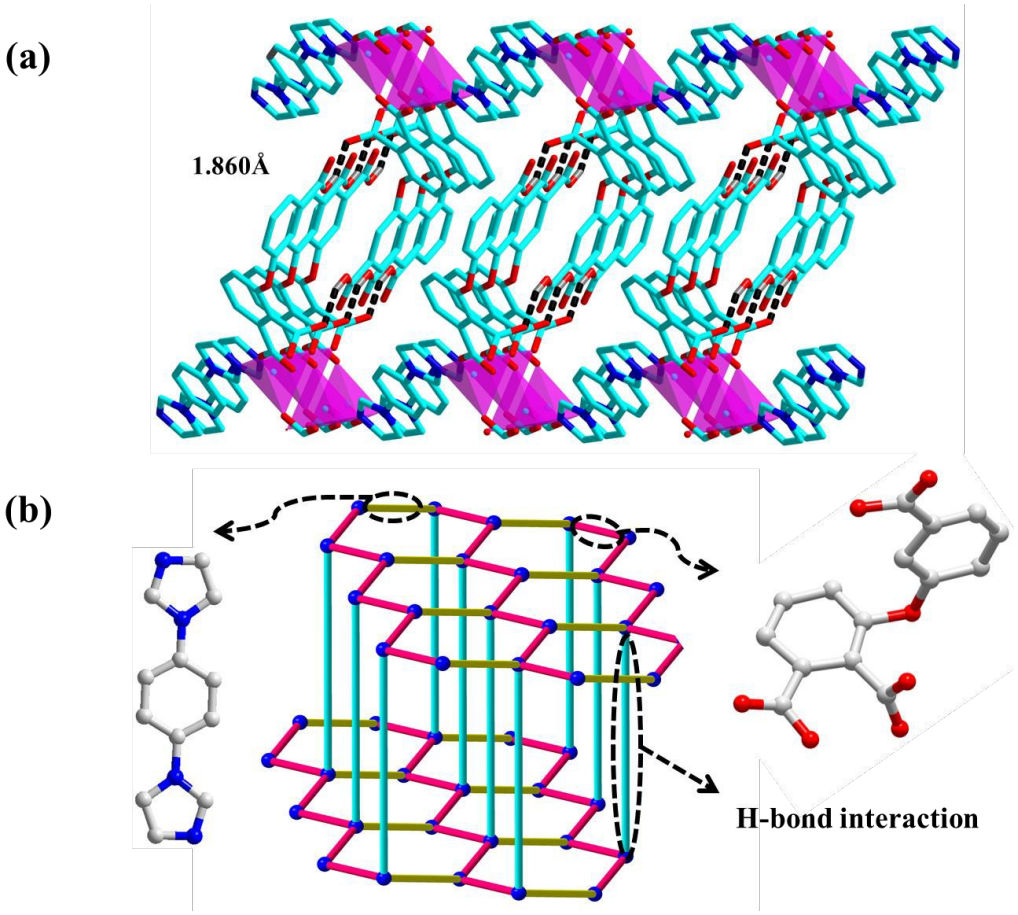

Fig. 5 (a) Polyhedral and stick representation of the 3D supramolecular structure of **3** (b) Topological view of the 3D structure of **3** with the 5-connected **bnn** net (color code: the zinc ions, blue ball; the defined linkers of bib and $Hdpob^{2-}$ ligand, yellow and rose sticks).

Although **3** possesses the same ligands as **2**, and their structures are similar, if we have deep insight to the building block of whole structure, the difference between **3** and **2** in the structure mainly focuses on the coordination mode in $Hdpob^{2-}$ and the relative position of H_3dpob and bib ligands. Concerning coordination mode of carboxyl group, that in **2** , by contrast, make metal center arrange more closer and better linear and 2D layer a flat one, instead of a wavelike one in **3**. About the two kinds of ligands' relative position in space, the plane of phthalandione is perpendicular to bib ligand in **2** and dihedral angle is 82.126° (Fig. 10d), but they show the parallel style in **3** with the value is 5.397° (Fig. 11d). Doubtfully, the differences we mentioned above have very closely relationship to the nature of metal centers in the process of constructing architecture.

{[$Cd_{1.5}$(dpob)(2,2′-bipy)]·0.5H_2O}$_{2n}$ (4) Coordination polymer **4** crystallizes in the chiral space group *C*222(1). There are two kinds of crystallographically independent Cd(II) ions. Cd1 ion is in an octahedral coordination environment built from six oxygen atoms from carboxyl groups in the monodentate and oxygen bridge coordination mode (Fig. S4a). Cd2 ion locates in a single-capped octahedral coordination sphere with two nitrogen atoms of 2,2′-bipy ligands occupying the two neighboring positions and four oxygen atoms at remaining positions from carboxyl groups in a monodentate and chelating mode (Fig. S4b). Through the Cd1 ion [site occupancy factor (SOF) = 0.5] as an inverse center, a linear trinuclear Cd subunit is formed by two crystallographically equivalent Cd2 and Cd2A ions in terminal positions and one Cd1 ion in the middle position (Fig. 6a). The neighboring trinuclear subunits are further connected by 3-carboxyl groups coordinating to Cd1 and Cd2(A) ions, forming a 2D layer in *ab* plane, as show in Fig. 6b. Notwithstanding, in coordination polymer **4**, three carboxyl groups of H_3dpob are all deprotonated, the occupied effect of chelating ligand 2,2′-bipy deters from a higher dimensional structure further.

The homochirality in the structure of **4** is worth noting. In **4**, the two phenyl rings of $dpob^{3-}$ ligand are in a nonplanar fashion (torsion angles is 77.7°), forming to

right-handed helices (Fig. 6c). The resulting right-handed helices with a pitch of 13.784 Å are alternately arranged in an equal ratio, extending into a 2D layer structure. The 1D helical infinite chains may be the origin of chirality in **4**. Solid-state circular dichroism (CD) measurements were performed on solid material in KBr plates to illustrate the chiral nature of **4**, and groups of randomly selected single crystals of **4** were used for the CD spectrum. As shown in Fig. S5, it exhibits an obvious Cotton effect with a positive CD signal,[35, 36] revealing that the entire bulk sample of **4** is a same handed conformation or may be racemic. The Flack parameter of **4** is -0.021(19), which further demonstrates the validity of the absolute configuration.

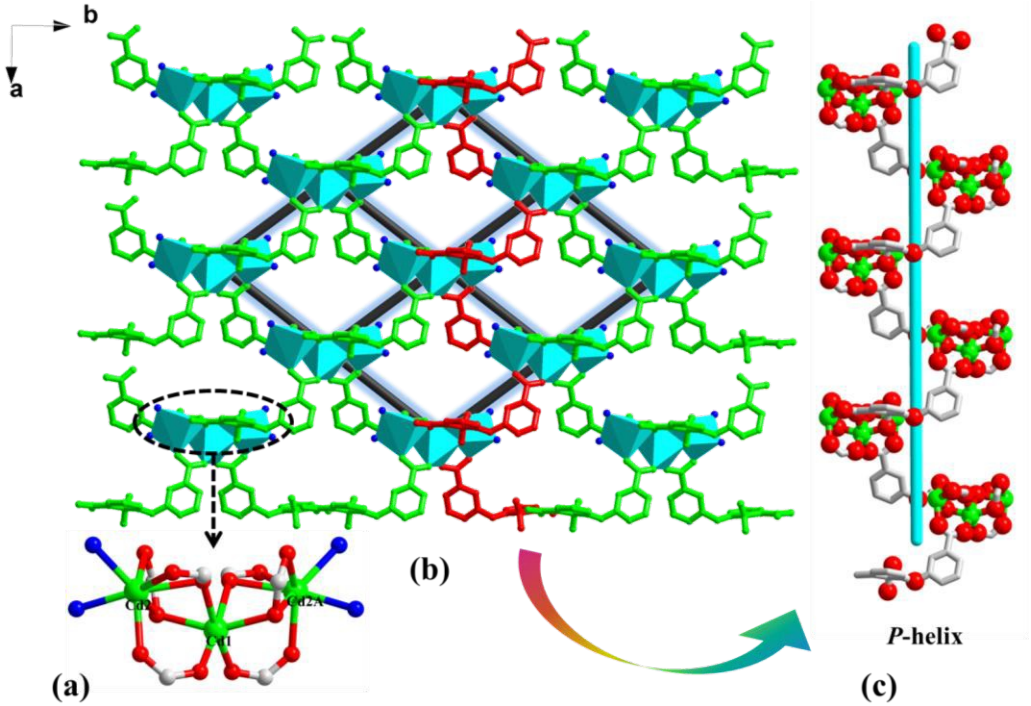

Fig. 6 (a) Trinuclear cluster structure and the coordination environments of the Cd^{2+} ions in **4**. Symmetry codes A: *x, -y, -z*. (b) The illustration of 2D grid layer of **4** in *ab* plane. (c) It shows a 1D right-handed helical infinite chain in **4**. (hydrogen atoms are omitted for clarity)

{[Cd_3(dpob)$_2$(4,4′-bipy)$_2$]·3H_2O}$_n$ (5) Single-crystal X-ray diffraction study indicates that coordination polymer **5** crystallizes in the triclinic *P*-1 space group, and its structure features a 3D pillared-layer like framework. In the asymmetric unit of **5**, there are three independent Cd(II) ions, all of which are different coordination environments. As shown in Fig. S6a, Cd1 and Cd2 both adopt distorted octahedral coordination geometry, the distinction is Cd1 completed by four carboxyl oxygen atoms from three different $dpob^{3-}$ ligands and two nitrogen atoms from two 4,4′-bipy

ligands, Cd2 is coordinated by five carboxyl oxygen atoms from four $dpob^{3-}$ ligands and one nitrogen atom from 4,4′-bipy ligand. Differently, Cd3 ion is seven-coordinated by six oxygen atoms from four $dpob^{3-}$ ligands and one nitrogen atom from 4,4′-bipy ligand resulting in the single-capped octahedral coordination geometry (Fig. S6b). Cd1, Cd2 and Cd3 are linked orderly *via* carboxylate groups, forming a trinuclear Cd_{oct}–Cd_{oct}–Cd_{hepta} secondary building unit (SBU). The 1D beaded chain generates from the connection of trinuclear clusters by $dpob^{3-}$ ligand coursing along [111] direction, and the coordination mode of $dpob^{3-}$ is same in each single bead (Fig. 7a). Furthermore, 4,4′-bipy ligands expand 1D chains to 3D window-like framework by bridge Cd1-Cd3 and Cd1-Cd2 (Fig. 7b). The trinuclear clusters as a SBU link four 4,4′-bipy ligands and four $dpob^{3-}$ ligands, in which one pair $dpob^{3-}$ anions are connected to the same trinuclear clusters, respectively, forming a closed-loop. In this way, the structure of **5** can be rationalized as a 6-connected **pcu** net with the Schläfli symbol of $\{4^{12}\cdot6^{3}\}$, as show Fig. 7c.

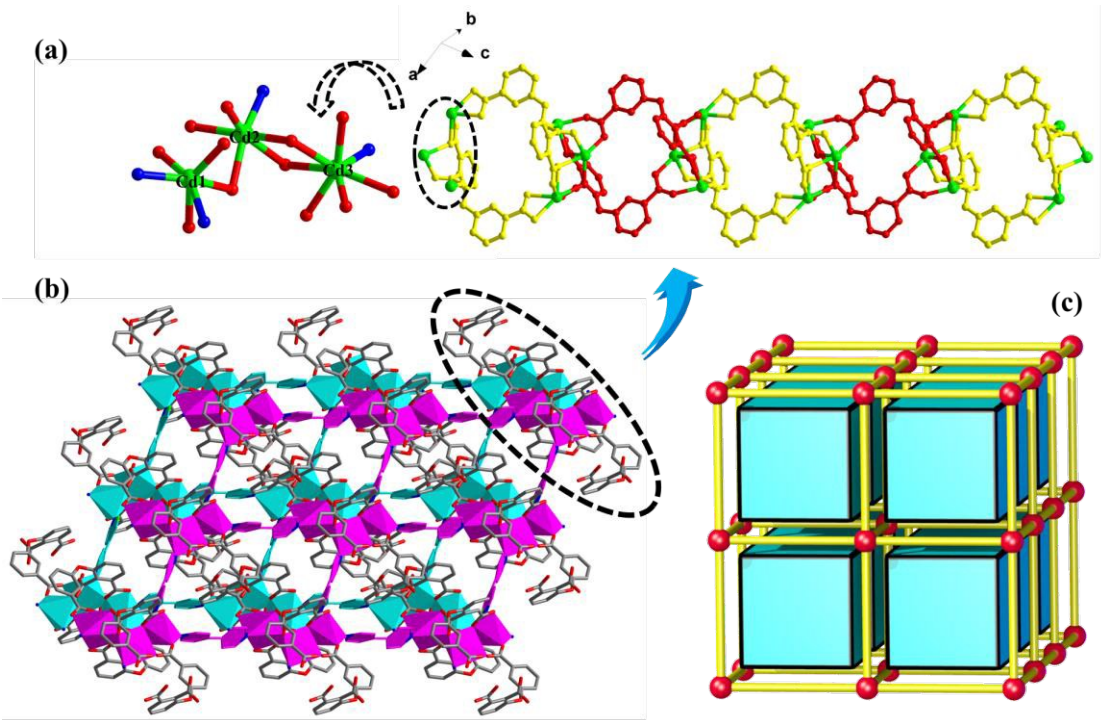

Fig. 7 (a) It shows trinuclear cluster structure and the coordination environments of the Cd^{2+} ions in **5**, and 1D beaded chain of **5** along [111] direction. (b) Polyhedral and stick representation of the 3D supramolecular structure of **5** (hydrogen atoms are omitted for clarity). (c) **pcu** topological net of **5**, with one kind of tiles (shown in blue) filling the space.

Coordination mode of the H_3dpob ligand induced by N-donor secondary ligands

Based on the discussion concerning the synthetic route above, it's easy to find the N-donor secondary ligands play key structure-directing roles in framework architecting. As excellent candidates to construct coordination polymers, asymmetric semirigid V-shaped multicarboxylate ligands, not only have diverse coordination mode and easily form a supramolecular structure *via* hydrogen bond interaction, but the twist of "centre O-atom" may increase complexity of configuration simultaneously as well. These points could be tuned by N-donor secondary ligands effectively. As a consequence, it seems necessary to reveal and understand the relationship between the coordination mode of carboxylic groups as well as conformation of ligands for the purpose of directional design and synthesis of functional coordination polymers. As can be seen in Scheme 2, five types of different coordination modes and two kinds of coordination configurations exist in **1**-**5**. Contrasting coordination modes among **1-3**, 3-carboxylic group in these three polymers are all undeprotonation. H_3dpob ligands show *trans*-coordination configuration with μ_2-η^1:η^1-syn,syn:syn connection mode in **1** (Scheme 2a). However, owing to introduce bib ligand to system, the positions of lattice water molecules have been replaced successfully, resulting that carboxylic ligands show μ_3-bridged modes in **2** (Scheme 2b) and **3** (Scheme 2c), but the connection modes are different. The connection mode in **2** is μ_3-$\eta^1\eta^1$:$\eta^2\eta^0$-syn,syn,anti:anti mode, and that of **3** is μ_3-$\eta^1\eta^1$:$\eta^1\eta^0$-syn,syn,anti:anti. In **5**, the length of auxiliary ligand is reduced with the coordinating points same, changing modes of H_3dpob ligand from μ_3 to μ_4 and μ_5 (Scheme 2e, 2f), both *cis*- and *trans*-typed configurations have been observed for each connection, which generate 1D beaded chain in final. Under the impact of chelating 2,2′-bipy, the carboxylic ligand in **4** only processes μ_5 bridging mode similar to that in **5** (Scheme 2d), but only *trans*-configuration. Additionally, hindrance of N-donor in space, the helix chain can be produced. Obviously, the structural diversity caused by coordination modes and configurations of H_3dpob can be indirectly influenced and tuned *via* controlling the natural aspects of N-donor auxiliary ligand.

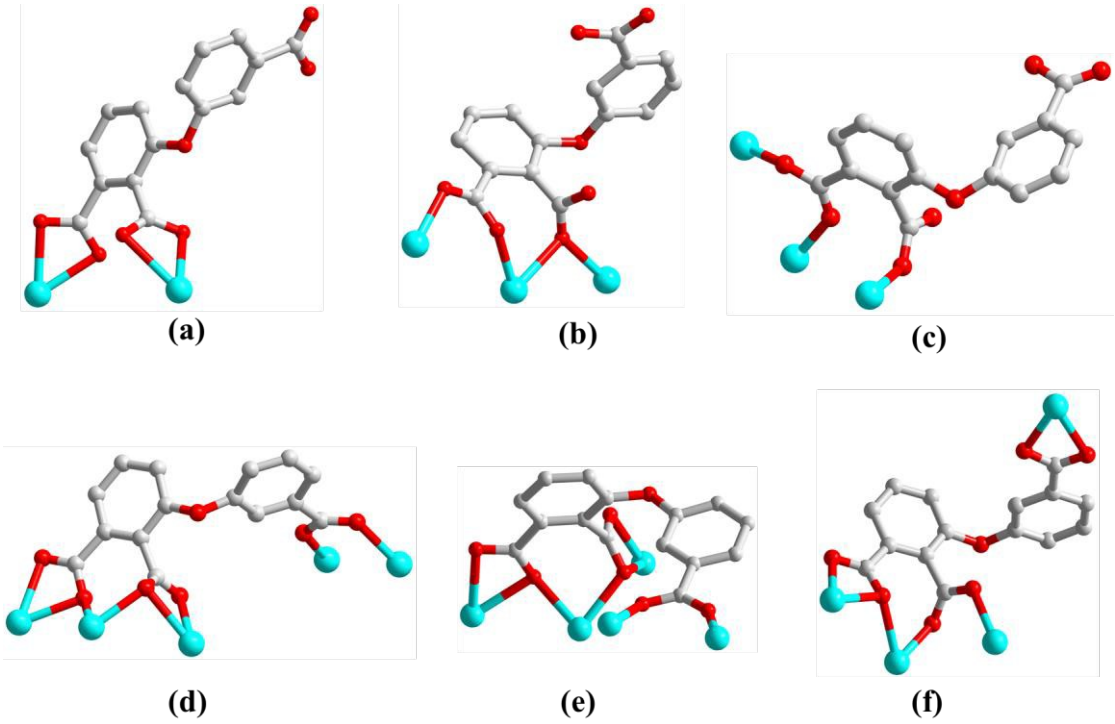

Scheme 2. Coordination modes and configuration of H3dpob ligands in coordination polymers **1**–**5**.

PXRD and thermal analyses

To check the phase purity of the products, powder X–ray diffraction (PXRD) experiments have been carried out for coordination polymers **1**–**5** (Fig. S8). The peak positions of the experimental and simulated PXRD patterns are in good agreement with each other, indicating that the crystal structures are truly representative of the bulk crystal products. To estimate the stability of the coordination architectures, thermogravimetric analyses (TGA) in purified air were carried out and the TGA curves are shown in Fig. S9. For **1**, the first weight loss from room temperature to 320 °C is consistent with the removal of four lattice water molecules (found 13.88 %, calcd 14.86 %). Afterwards the collapse of the network of **1** occurs. For **2**, the TGA curve displays one continuous weight loss step from 305 °C (found 20.05 %, calcd 20.55 %), which is attributed to the decomposition of the framework. The TGA curve of **3** shows one-step weight loss process from 340 to 500 °C, corresponding to the collapse of the framework (found 17.93 %, calcd 17.29 %). Host framework of coordination polymer **4** could keep until 350 °C and the rapid weight loss occurs from 350 to 425 °C owing to the decomposition of organic ligands. After further heating,

the TGA curve keeps horizontal. Coordination polymer **5** shows the first weight loss of 3.55 % from 30 to 270 °C, which is consistent with the removal of three water molecules (calcd 4.15 %), and then the whole structure starts to collapse. The remaining residue of five coordination polymers is consistent with the formation of the corresponding metal oxides, respectively.

Luminescence properties

The d^{10} coordination polymers and conjugated organic linkers have attracted much interest for their potential applications as photoactive materials.[37, 38] Hence, the luminescent properties of coordination polymers **1**-**5**, together with all the free organic ligands, have been investigated in the polar solvent dimethyl sulfoxide (DMSO) with the concentration of 1.0×10^{-5} mol/L at room temperature. The ^{1}H NMR and HRMS (ESI) data indicate that **1**-**5** still keep a polymeric structure in DMSO solution and do not decompose (Fig. S10 and Fig. S11). The two main absorption bands in UV spectra (Fig. S12) can be attributed to ligand-centered $\pi \rightarrow \pi^*$ transition. We further examined the quantum yields (Φ) to DMSO with the same concentration at 298 K, corresponding data are listed in Table S2.

As shown in Fig. 8, in DMSO at 298 K, coordination polymers **1**-**5** all show two emission bands and display deep blue, jewelry blue, light blue, green-blue and green luminescence emissions with CIE (Commission Internacionale d′Eclairage) coordinates in DMSO. The two emission bands may be both assigned to the ligand-centered $\pi^* \rightarrow \pi$ transitions with a slight disturb of metal center ions, due to those similarity to H_3dpob (Fig. S13).[39, 40] Among four cases of Cd coordination polymers, the high-energy emission (HE) of **1** and **5** are roughly same as that of ligand, but they both showing the relative enhancement effect to the low-energy emission (LE) with identical degree. Differently, **4** makes the HE bathochromic shift, and nearly do not change the intensity of LE instead. Comparably, the HE of **2** demonstrates maximum red-shift following the dramatically enhancement to LE band. However, for Zn coordination polymer, **3** keeps the position of HE basically same and shows intensity-quenching effect to LE. Obviously, after constructing coordination

polymers with participation of metal ions, the different extent changes, comparing to ligand, have happened to emission spectrum, particularly, the difference focused on LE is clear enough. Generally speaking, that phenomenon could be assigned to the structural complexity and framework robustness.[41] It is worthy to note that **2** and **3** are constructed by same ligands and display similar structure, nevertheless, the intensity of LE in **2** and **3**, respectively, is the highest and lowest among the series of coordination polymers. The huge difference attracts our passion to search for the internal reason.

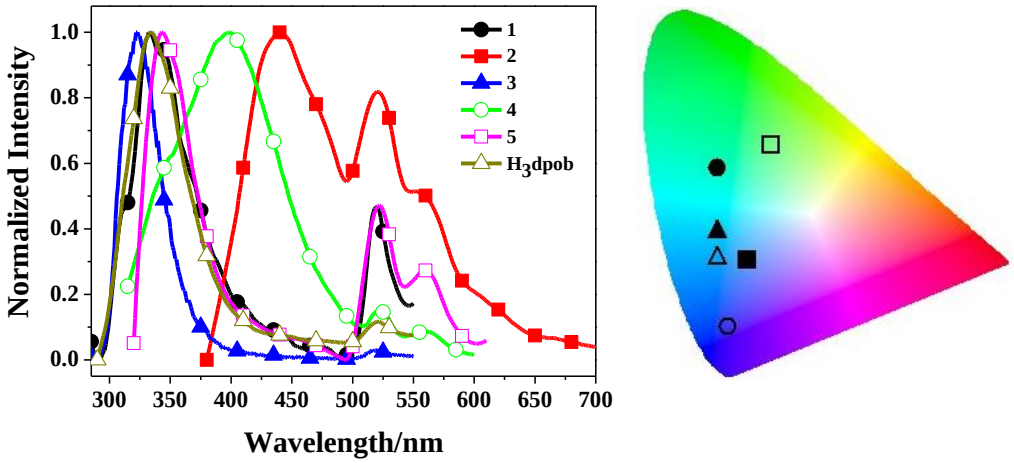

Fig. 8 Normalized emission spectra of coordination polymers **1**–**5** in DMSO solution (concentration: 10^{-5} M) at 298 K and the corresponding color coordinate diagram of emission (the color circle corresponding with the lines).

To dual-emissive materials, luminescence response behavior may be more sensitive to outside environment, such as variation of excitation light. Within **2** and **3**, the outstanding discrepancy is central metals. Hence, we may make assumption that the difference of LE intensity in **2** and **3** originate from the perturbation effect of central metals. We choose **2** and **3** to further investigate the influence by variation of excitation light. When excited by 330 nm light, the green LE band ~520 nm is much brighter than the blue HE band ~440 nm for **2**. As shown in Fig. 9a, the increase of the wavelength of excitation light at a step of 10 nm outstandingly reduces the relative intensity of the LE peak but slightly enhances the HE band. When excited at 370 nm, the contribution of the HE band dominates the total emission spectrum. Correspondingly, the luminescence of **2** is tunable from green to blue light based on

excitation wavelength ranging from 330 to 370 nm (Fig. 9b). Similar to **2**, the luminescent spectra of **3** also contains two groups of peaks and relative intensity of two peaks changes with variation of excitation light as well, but different from **2**, upon excitation in the range of 280–320 nm, the evidently reduce of HE band is observed. Comparatively speaking, the intensity of LE band enhances slightly (Fig. 10a). Considering those from integrated intensity of emission peaks perspective (Table S3), though HE and LE of **2** decrease meanwhile at different speed (inset picture of Fig. 11a) and inset picture of Fig. 10a shows HE minishes dramatically following that of LE enhance, the final tendency and color reached are determined by predominant peak. Combining the interaction between HE and LE bands, a rule of color-tuned visually reflects in CIE coordinates (Fig. 9b and 10b), corresponding data are listed in Table S4.

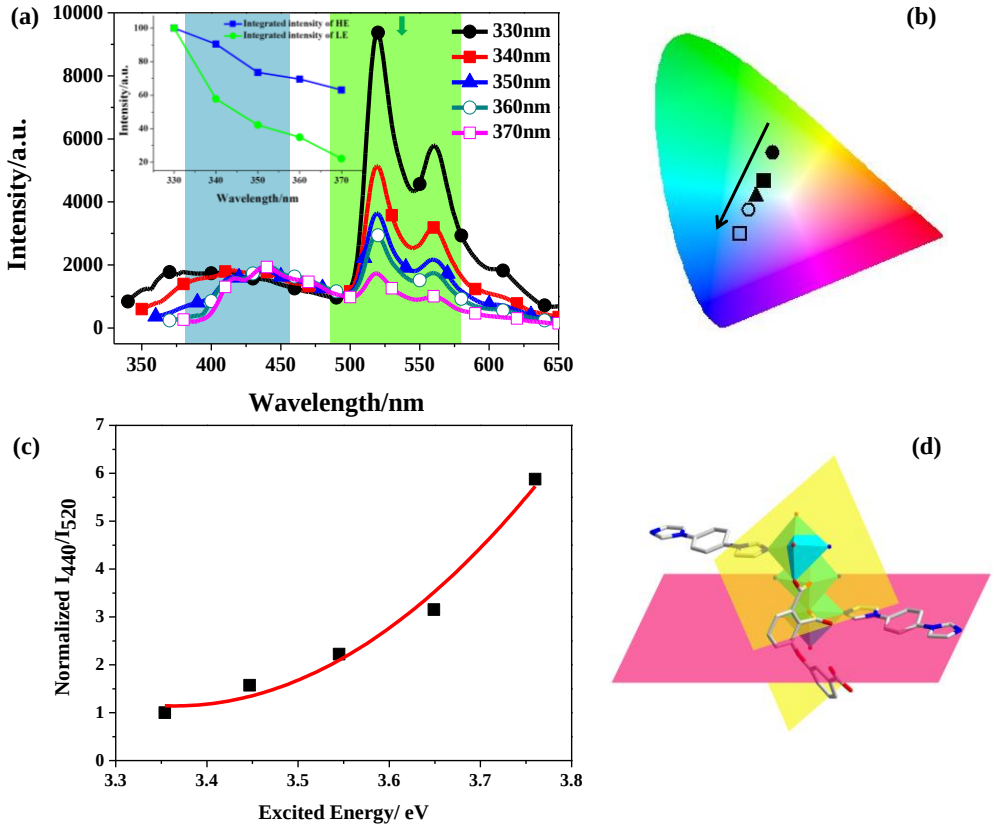

Fig. 9 (a) Emission spectra of **2** in DMSO solution by varying the excitation light wavelength under the same metrical conditions (slit width: 1 nm, 1 nm), Inset: corresponding integrated intensity of HE (440 nm) and LE (520 nm). (b) The corresponding color coordinate diagram shows the tunable green-to-blue luminescence of **2**. (c) Excited energy-dependent intensity ratio of HE to LE and the fitted curve for **2**. (d) Vertical configuration between H_3dpob and bib ligands shows in **2**.

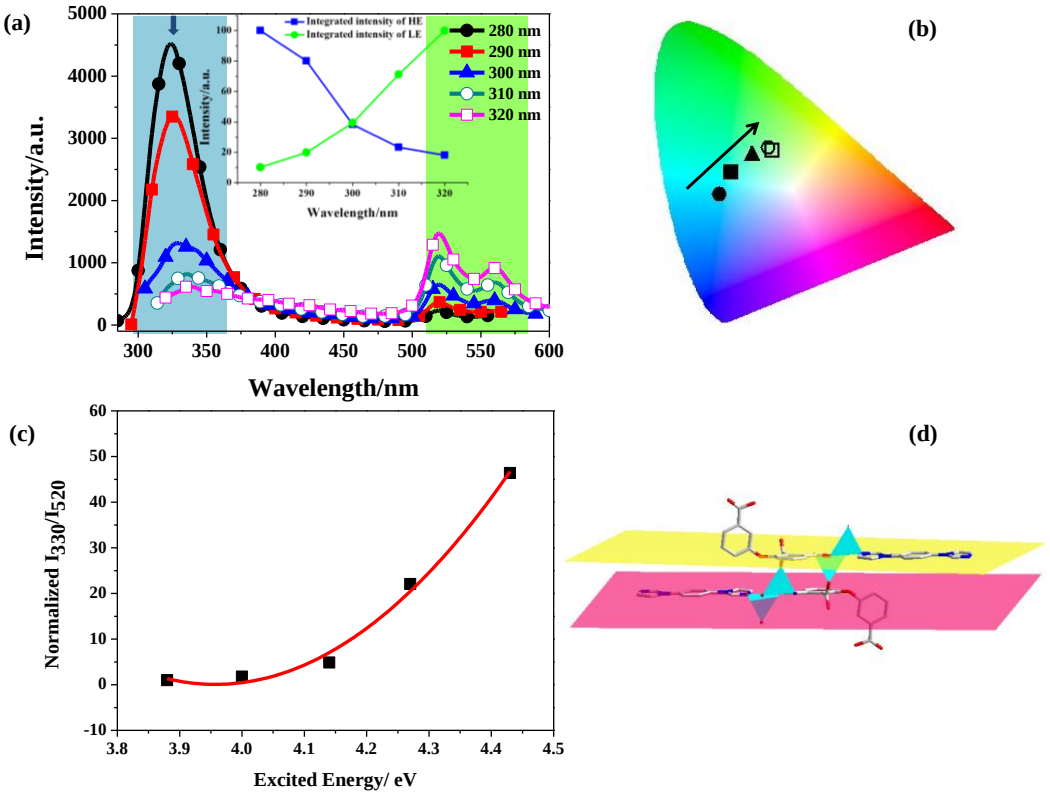

Fig. 10 (a) Emission spectra of **3** in DMSO solution by varying the excitation light wavelength under the same metrical conditions (slit width: 1 nm, 1 nm), Inset: corresponding integrated intensity of HE (330 nm) and LE (520 nm). (b) The corresponding color coordinate diagram showing the tunable blue-to-green luminescence of **3**. (c) Excited energy-dependent intensity ratio of HE to LE and the fitted curve for **3**. (d) Parallel configuration between H_3dpob and bib ligands shows in **3**.

Remarkably, the exactly opposite tunable tendency, for **2** and **3**, can be associated the following factors: (i) Different metal center. The zinc has smaller radius and superior binding capacity for surrounding electrons. This leads to the larger π-conjugated electrons of ligands system go on stronger luminescent response. Namely, the ligand-centered transition is dominant and the HE emission band is more sensitive to excitation energy. Cd-center coordination polymer **2**, the electrons of metal component show the greater degree of freedom and more easily conduct and flow in structure, naturally, the change of emissive band generating from the disturb of metal center ions is increasingly obvious. (ii) Individual coordination environment. The relative position of H_3dpob and bib show two categories in space: verticality for **2** and parallel for **3** respectively. The whole structural degree of delocalization in **3** is larger than that in **2**, which is beneficial to the π*→π electron transition. For **2**, owing

to the coordination environment of cadmium atom, main ligand and N-donor ligand show vertical mode. Additionally, the seven-atom chair-like circle (Fig. S18) which consists of metal center and carboxyls of phthalandione make the cadmium ion easier to disturb the LE band.

Though, the difference originate from metal center, specific to luminescence property, the irritability to surrounding may differ to each other. To measure tunable-sensitivity to energy quantitatively between **2** and **3**, we consider introduce the concept of relative sensitivity.[42] Fig. 9c plots the ratio of the two luminescence intensity at HE (~440 nm) and LE (~520 nm) of **2** versus excitation energy, normalized to this intensity ratio at 3.354 eV. There is a good quadratic polynomial relationship between the intensity ratio and excitation energy, which can be fitted as a function of

$$I_{440}/I_{520} = 332.86 - 197.19(E) + 29.31(E)^2 \quad (1)$$

with correlation coefficient 0.967, where I_{440} and I_{520} are the luminescence intensity of HE and LE, respectively, E is the excitation energy of the detection system (eV). Same mathematical processing are handled for **3**, normalized to the intensity ratio at 3.880 eV, the relationship between intensity ratio and excitation energy can be fitted as a function of

$$I_{330}/I_{520} = 3309.78 - 1672.07(E) + 211.18(E)^2 \quad (2)$$

with correlation coefficient 0.988 (Fig. 10c). Obviously, the excellent sensitivity of **2** and **3** are both located at relative high excitation energy region, which is in agreement with emission spectra of **2** and **3** respectively. The relative sensitivity is usually utilized and defined as

$$S = \frac{\partial(P)/\partial E}{P} \quad (3)$$

where P is the measured energy-sensitive parameter, such as intensity, lifetime, or intensity ratio.[43] For energy-sensitivity of **2** and **3**, the relative sensitivity can be determined as

$$S = \frac{\partial(I_1/I_2)/\partial E}{I_1/I_2} \quad (4)$$

where I_1 and I_2 are the two luminescence intensities of the dual emission. [44, 45] Following the definition, the maximum sensitivity of **2** is determined to be 3.95% eV^{-1}, which is a little lower than the sensitivity achieved from **3** (4.29% eV^{-1}). Calculations from signal-to-noise ratios by a modern fluorescence spectrometer show that a 0.02% change of intensity ratio can be readily measured,[42] which means that the theoretical maximum excited-energy sensing resolution of **2** and **3** could be better than 0.005 and 0.004 eV.

The emission spectrum of solid-state samples of coordination polymers in this work are centered at 414 nm for **1**, 410 nm for **2**, 403 nm for **3**, 380 nm for **4** and 515 nm for **5**, displaying deep blue, light blue and green luminescent emissions with CIE coordinates (Fig. 11). Comparing to the emissions in DMSO solvent, it's easy to find **1-5** and H_3dpob show the single peaks with the LE bands absence. That's might be assign to the aggregation effect in the solid state, further leading the refined-structure missing in the spectra.[46] Setting H_3dopb ligand as reference, red shifts of emission bands for **1-3** and **5** (18 , 14 , 7 and 119 nm) have been observed, while the emission band of **4** presents a slightly blue shift (16 nm) (Fig. S14). The different luminescence behaviors of **1-5** may be due to various coordinated modes of H_3dpob and distinct N-donor co-ligands, which may affect the rigidity of the whole framework and further influence their luminescence emission bands in the solid state.[47] The solid state luminescence spectra of **1-5** at liquid nitrogen temperature are researched as well. Obviously, when temperature decreases to 77 K, a huge bathochromic shift of emission peaks of **1-5** happened in the solid state (61 nm for **1**, 150 nm for **2**, 123 nm for **3**, 207 nm for **4**, 75 nm for **5**), which results **2**, **4**, and **5** dropping in yellow light region (at the edge of CIE chromaticity diagram as show in Fig. 11). The shift in luminescence spectra at low temperatures so called "luminescence thermochromism" is usually explained by predomination "cluster centred".[48-50] By contrast, the red shift degree of **1** and **5** is smaller, due to the fact that existence of more water molecules, to some extent, may increase the radiationless transition.[51] The luminescent lifetimes of **1–5** increase to those at 298 K (298 K: τ = 7.37 μs, 7.56 μs, 7.68 μs, 6.82 μs, 5.80 μs for **1–5**; 77 K: τ = 7.77 μs, 8.91 μs, 9.90 μs, 8.74 μs, 7.69 μs for **1–5**) (Table. S2),

since cold conditions would be favorable to the rigidity of ligands with reducing the non–radiation decay and collisional quenching.[52, 53]

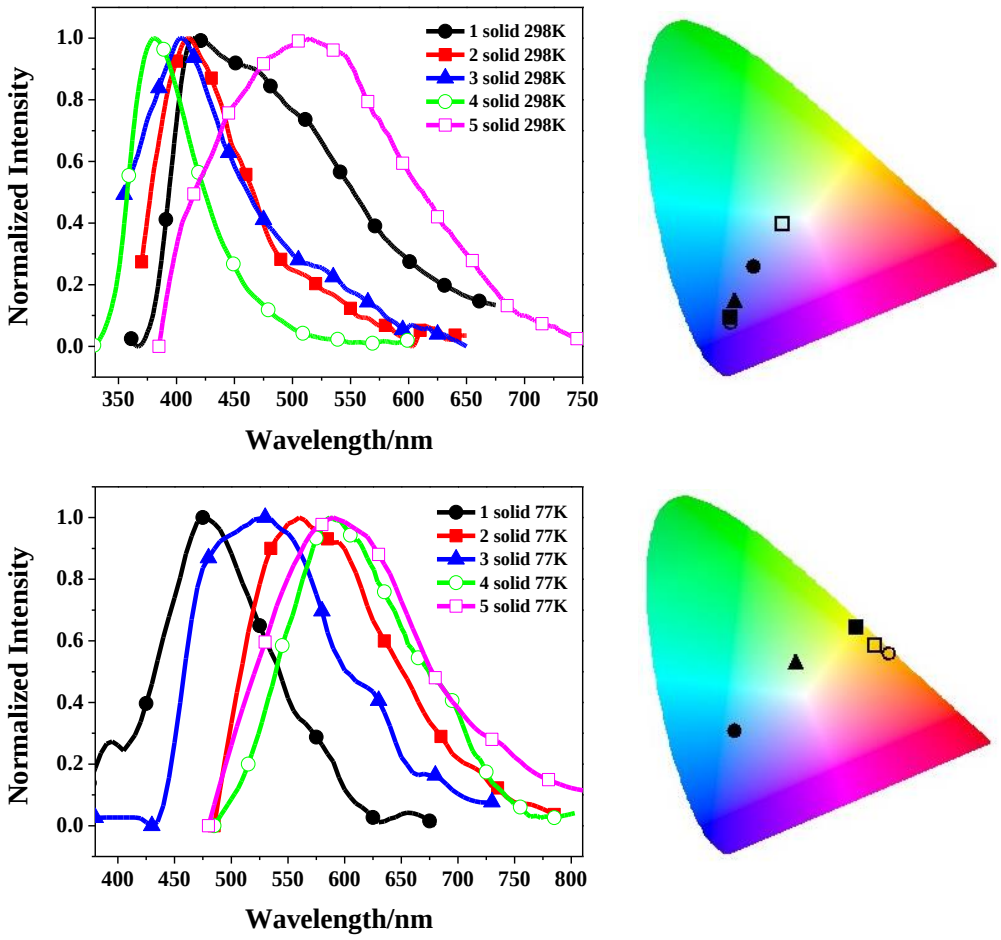

Fig. 11 Normalized emission spectra of **1**–**5** at 298 K, 77 K in solid state and the corresponding color coordinate diagram of emission.

Conclusion

In summary, five zinc/cadmium (II)- 3-(2′,3′-Dicarboxylphenoxy)benzonic acid coordination polymers with a variety of one-, two-, and three dimensional architectures have been synthesized with the help of a series of rationally selected N-donor ligands. Structural comparisons of these five coordination polymers illustrated that N-donor secondary ligands held dominating advantage competing with water molecules, and final structure can be determined by reasonable control of the detailed morphological factors of themselves. Coordination polymers **1-5** all display dual-emission response sensitivity of DMSO. Remarkably, **2** and **3** constructed by same ligands with similar structure make the huge different contribution to LE, which may originate from the difference of metal center. Furthermore, emissive light of **2** and **3** can be tuned between blue and green varying the excitation wavelength, and the

tuning tendency can be tailored with opposite directions. In the solid state at room temperature, the coordination polymers display blue and green luminescence and the change of temperature from 298 K to 77 K caused a hypochromatic shift of emission peaks. The brilliant luminescence properties make coordination polymers **1-5** promising material for the development of optical devices. It may bring out a new strategy to specific secondary regulating in controllable synthesis of the dual-emissive materials and deeper thinking concerning luminescent behavior.

Experimental section

Materials and methods

All reagents were commercially available and used without further purification. IR spectra were obtained from KBr pellets, using a Nicolet Avatar-360 Infrared spectrometer in the 4000–400 cm^{-1} region. Elemental analyses were performed on a Perkin-Elmer 240c element analyzer. Powder X-ray diffraction (PXRD) patterns were recorded in the 2θ range of 5–50° using Cu Kα radiation by Shimadzu XRD-6000 X-ray Diffractometer. The thermal analysis was performed on a ZRY-2P thermogravimetric analyzer from 25 to 700 °C with heating rate of 10 °C min^{-1} under a flow of air. ^1H NMR spectra were recorded on a Bruker ACF 400 MHz at room temperature. HRMS (ESI) spectra were recorded on a Bruker Esquire LC mass spectrometer using electrospray ionization in DMSO. UV spectra were obtained on a Perkin-Elmer Lambda 20 spectrometer. Luminescence analysis and luminescence lifetimes were recorded on Edinburgh FLS920 luminescence spectrometer at 298 K and 77 K. The luminescence quantum yields of complexes were measured in DMSO at room temperature and cited relative to a reference solution of quinine sulfate (Φ = 0.546 in 0.5 mol dm^{-3} H_2SO_4) as a standard, and they were calculated according to the well-known equation (a): $\frac{\varphi_{overall}}{\varphi_{ref}} = \left(\frac{n}{n_{ref}}\right)^2 \frac{A_{ref}}{A}\frac{I}{I_{ref}}$ (a). In equation (a), n, A, and I denote the refractive index of solvent, the area of the emission spectrum, and the absorbance at the excitation wavelength, respectively, and φ_{ref} represents the quantum yield of the standard quinine sulfate solution. The subscript ref denotes the reference, and the absence of a subscript implies an unknown sample. For the determination of

the quantum yield, the excitation wavelength was chosen so that A < 0.05.

Synthesis of {[Cd(Hdpob)(H_2O)$_3$]·H_2O}$_n$ (1)

A mixture of $Cd(NO_3)_2$·$4H_2O$ (61.6 mg, 0.2 mmol), H_3dpob (30.2 mg, 0.1 mmol) were dissolved in CH_3CN (2.0 mL) and H_2O (6.0 mL), and stirred in air for 20 min, and then heated in a 20.0 mL Teflon-lined stainless steel autoclave at 120 °C for 4 days under autogenous pressure. After cooling to the room temperature, colorless rectangular block crystals of **1** were obtained (yield, 43 %, based on H_3dpob). Anal. Calcd. For $C_{15}H_{16}O_{11}Cd$ (Mr: 484.68): C, 37.17; H, 3.32. Found: C, 37.12; H, 3.35. IR (KBr pellet, cm^{-1}) for **1** (Fig. S7): 3338 (br, s), 2501 (w), 1700 (s), 1581 (s), 1540 (s), 1483 (s), 1402 (s), 1288 (s), 1220 (w), 1251 (s), 1220 (w), 989 (m), 871 (m), 821 (m), 773 (m), 750 (m), 692 (w), 657 (w), 534 (w), 443(w). ^{1}H NMR (400 MHz, DMSO–d_6, Fig. S10): δ = 13.64 (s, 1 H, -COO*H*), 7.78 (d, 1 H, Ph–H_{13}), 7.70 (d, 1 H, Ph–H_5), 7.48 (t, 2 H, Ph–$H_{14,15}$), 7.40 (s, 1 H, Ph–H_2), 7.24 (d, 1 H, Ph–H_6), 7.19 (s, 1 H, Ph–H_7) ppm. HRMS (ESI) for **1** (Fig. S11): m/z = 122.0567 $[Ph\text{-}COOH + H]^+$, 423.1988 $[M - COOH - 2H_2O + H]^+$, 489.6129 $[M - 2H_2O + Na]^+$.

Synthesis of [Cd(Hdpob)(bib)]$_n$ (2)

A mixture of $Cd(NO_3)_2$·$4H_2O$ (77.0 mg, 0.25 mmol), H_3dpob (30.2 mg, 0.1 mmol) and bib (10.5 mg, 0.05 mmol) were dissolved in CH_3OH (2.0 mL) and H_2O (6.0 mL), and stirred in air for 20 min, adjusting the pH to 6 by addition of 0.1 M NaOH solution, and then transferred into a 20.0 mL Teflon-lined stainless steel autoclave and heated at 120ºC for 4 days under autogenous pressure. After cooling to the room temperature, colorless block crystals of **2** were obtained (yield, 62 %, based on bib). Anal. Calcd. For $C_{27}H_{18}N_4O_7Cd$ (Mr: 622.86): C, 52.07; H, 2.91; N, 9.00. Found: C, 52.04; H, 2.87; N, 9.04. IR (KBr pellet, cm^{-1}) for **2** (Fig. S7): 3157 (br, w), 3124 (w), 3091 (w), 1701 (s), 1566 (s), 1533 (s), 1493 (w), 1441 (m), 1389(m), 1309(m), 1244 (m), 1065 (m), 958(m), 933 (w), 883 (m), 783 (m), 762 (m), 644 (m), 596 (w), 455 (w). ^{1}H NMR (400 MHz, DMSO–d_6, Fig. S10): δ = 13.62 (s, 1 H, -COO*H*), 8.35 (s, 2 H, Imi–$H_{17,26}$), 7.84 (s, 2 H, Imi–$H_{16,25}$), 7.83 (d, 4 H, Ph–$H_{20,21,23,24}$), 7.76 (d, 1 H, Ph–H_{13}), 7.71 (d, 1 H, Ph–H_5), 7.51 (t, 2 H, Ph–$H_{14,15}$), 7.39 (s, 1 H, Ph–H_2), 7.28 (d,

1 H, Ph–H_6), 7.19 (s, 1 H, Ph–H_7), 7.15 (s, 2 H, Imi–$H_{18,27}$) ppm. HRMS (ESI) for **2** (Fig. S11): *m/z* = 122.0567 [Ph-COOH + H]$^+$, 623.3060 [M+ H]$^+$, 645.8652 [M + Na]$^+$, 433.7695 [M – Ph-COOH – im]$^+$.

Synthesis of [Zn(Hdpob)(bib)$_{0.5}$]$_n$ (3)

The preparation of **3** was similar to that of **2** except that $Cd(NO_3)_2{\cdot}4H_2O$ was replaced by $Zn(NO_3)_2{\cdot}6H_2O$ (74.0 mg, 0.25 mmol) as a starting material and colorless block crystals of **3** were obtained (yield, 58 %, based on bib). Anal. Calcd. For $C_{21}H_{13}N_2O_7Zn$ (Mr: 470.72): C, 53.58; H, 2.76; N, 5.95. Found: C, 53.52; H, 2.74; N, 5.97. IR (KBr pellet, cm^{-1}) for **3** (Fig. S7): 3435 (br, w), 3126 (w), 3063 (w), 1719 (s), 1601 (s), 1583 (s), 1564 (s), 1540 (s), 1471 (m), 1449 (m), 1407 (s), 1387 (s), 1327 (w), 1289 (m), 1247 (s), 1209 (m), 1104 (w), 1071 (s), 980 (m), 961 (m), 897 (w), 759 (m), 739 (m), 649 (m), 566 (w), 479(w). ^{1}H NMR (400 MHz, DMSO–d_6, Fig. S10): δ = 13.63 (s, 1 H, -COO*H*), 8.36 (s, 1 H, Imi–H_{17}), 7.84 (s, 1 H, Imi–H_{16}), 7.83 (d, 2 H, Ph–$H_{20,21}$), 7.77 (d, 1 H, Ph–H_{13}), 7.70 (d, 1 H, Ph–H_5), 7.51 (t, 2 H, Ph–$H_{14,15}$), 7.39 (s, 1 H, Ph–H_2), 7.28 (d, 1 H, Ph–H_6), 7.19 (s, 1 H, Ph–H_7), 7.15 (s, 1 H, Imi–H_{18}) ppm. HRMS (ESI) for **3** (Fig. S11): *m/z* = 122.1015 [Ph-COOH + H]$^+$, 425.4036 [M – COOH + H]$^+$, 454.2879 [M + 0.5 bib – Ph-COOH + H]$^+$, 598.3888 [M + 0.5 bib + Na]$^+$.

Synthesis of {[Cd$_{1.5}$(dpob)(2,2′-bipy)]·0.5H$_2$O}$_{2n}$ (4)

A mixture of $Cd(NO_3)_2{\cdot}4H_2O$ (61.6 mg, 0.2 mmol), H_3dpob (30.2 mg, 0.1 mmol), 2,2′-bipy (16.0 mg, 0.1 mmol) and NaOH (8.0 mg, 0.25 mmol) were dissolved in H_2O (10.0 mL), and stirred in air for 20 min, and then heated in a 20.0 mL Teflon-lined stainless steel autoclave at 160 °C for 4 days. After cooling to the room temperature, obtained colorless crystals **4** (yield, 56 %, based on H_3dpob), the shape of them were like a combination of quadrangular and the four pyramid. Anal. Calcd. For $C_{50}H_{31}N_4O_{15}Cd_3$ (Mr: 1265.02): C, 47.47; H, 2.47; N, 4.43. Found: C, 47.49; H, 2.43; N, 4.40. IR (KBr pellet, cm^{-1}) for **4** (Fig. S7): 3417 (br, w), 1643 (m), 1552 (s), 1471 (m), 1382 (s), 1311 (w), 1290 (w), 1267 (m), 1247 (s), 1218 (w), 1191 (w), 1157 (w), 1105 (w), 1105 (w), 1060 (w), 1018 (m), 985 (m), 900 (m), 848 (m), 819 (m), 761 (s),

626 (m), 592 (w), 493 (w). ^{1}H NMR (400 MHz, DMSO–d_6, Fig. S10): δ = 8.72 (s, 2 H, Py–$H_{17,22}$), 8.41 (s, 2 H, Py–$H_{20,25}$), 7.97 (t, 2 H, Py–$H_{18,23}$), 7.75 (d, 1 H, Ph–H_{13}), 7.68 (d, 1 H, Ph–H_5), 7.50 (t, 2 H, Ph–$H_{14,15}$), 7.48 (t, 2 H, Py–$H_{19,24}$), 7.40 (s, 1 H, Ph–H_2), 7.28 (d, 1 H, Ph–H_6), 7.20 (s, 1 H, Ph–H_8) ppm. HRMS (ESI) for **4** (Fig. S11): *m/z* = 623.3117 $[0.5(M – H_2O) + H]^+$, 634.8954 $[M – 2bipy – H_2O – dpob]^+$, 934.4718 $[M – 2bipy – H_2O + H]^+$.

Synthesis of $\{[Cd_3(dpob)_2(4,4'\text{-bipy})_2]\cdot 3H_2O\}_n$ (5)

The preparation of **5** was similar to that of **4** except that 2,2′-bipy was replaced by 4,4′-bipy (16.0 mg, 0.1 mmol) as a starting material and colorless block crystals of **5** were obtained (yield, 64 %, based on H_3dpob). Anal. Calcd. For $C_{50}H_{36}N_4O_{17}Cd_3$ (Mr: 1302.06): C, 46.12; H, 2.79; N, 4.30. Found: C, 46.17; H, 2.73; N, 4.25. IR (KBr pellet, cm^{-1}) for **5** (Fig. S7): 3434 (br, m), 3058 (w), 1641 (m), 1605 (s), 1563 (s), 1486 (m), 1473 (m), 1434 (m), 1396 (s), 1314 (m), 1291 (m), 1227 (m), 1253 (s), 1226 (m), 1203 (m), 1141 (w), 1115 (w), 980 (m), 859 (w), 804 (m), 778 (m), 738 (w), 622 (m), 565 (w), 486 (m). ^{1}H NMR (400 MHz, DMSO–d_6, Fig. S10): δ = 8.73 (d, 8 H, Py–$H_{12,15,17,24,50,63,65,70}$), 7.85 (s, 8 H, Py–$H_{4,6,9,11,51,62,64,66}$), 7.78 (d, 2 H, Ph–$H_{5,25}$), 7.71 (d, 2 H, Ph–$H_{19,26}$), 7.51 (t, 4 H, Ph–$H_{1,2,3,13}$), 7.40 (s, 2 H, Ph–$H_{21,23}$), 7.27 (d, 2 H, Ph–$H_{16,29}$), 7.22 (s, 2 H, Ph–$H_{8,36}$) ppm. HRMS (ESI) for **5** (Fig. S11): *m/z* = 157.0754 $[bipy + H]^+$, 423.2016 $[0.5(M – 3H_2O) – bipy – COOH + H]^+$, 792.8534 $[M – 3H_2O – bipy – dpob]^+$.

X-Ray crystal structure determination

The X-ray diffraction data taken at room temperature for coordination polymers **1**–**5** were collected on a Rigaku R-AXIS RAPID IP diffractometer equipped with graphite-monochromated Mo Kα radiation (λ = 0. 71073 Å). The structures of **1**–**5** were solved by direct methods and refined on F^2 by the full-matrix least squares using the SHELXTL-97 crystallographic software.[54, 55] Anisotropic thermal parameters are refined to all of the non-hydrogen atoms. The hydrogen atoms were held in calculated positions on carbon atoms and nitrogen atoms and that were directly included in the molecular formula on water molecules. The CCDC 1401569, 1401570, 1401571,

1401572 and 1401573 contain the crystallographic data **1**–**5** of this paper. These data can be obtained free of charge at www.ccdc.cam.ac.uk/ deposit. Crystal structure data and details of the data collection and the structure refinement are listed as Table 1, selected bond lengths and bond angles of coordination polymers **1**–**5** are listed as Table S6

Acknowledgements

This work was supported by National Natural Science Foundation of China (Grant 21371040, 21571042 and 21171044), the National key Basic Research Program of China (973 Program, No. 2013CB632900), supported by the Fundamental Research Funds for the Central Universities (Grant No. HIT. IBRSEM. A. 201409).

References

1. L. N. Li, S. Q. Zhang, L. Han, Z. H. Sun, J. H. Luo and M. C. Hong, *Cryst. Growth Des.*, 2013, **13**, 106-110.
2. X. C. Shan, F. L. Jiang, D. Q. Yuan, H. B. Zhang, M. Y. Wu, L. Chen, J. Wei, S. Q. Zhang, J. Pan and M. C. Hong, *Chem. Sci*, 2013, **4**, 1484-1489.
3. X. Zhang, T. Xie, M. Cui, L. Yang, X. Sun, J. Jiang and G. Zhang, *ACS Appl. Mater. Inter*, 2014, **6**, 2279-2284.
4. G. Zhang, G. M. Palmer, M. W. Dewhirst and C. L. Fraser, *Nat. Mater*, 2009, **8**, 747-751.
5. Q. Zhao, X. B. Zhou, T. Y. Cao, K. Y. Zhang, L. J. Yang, S. J. Liu, H. Liang, H. R. Yang, F. Y. Li and W. Huang, *Chem. Sci*, 2015, **6**, 1825-1831.
6. K. Honda, S. H. Fujishima, A. Ojida and I. Hamachi, *ChemBioChem*, 2007, **8**, 1370-1372.
7. X. H. Jin, C. X. Ren, J. K. Sun, X. J. Zhou, L. X. Cai and J. Zhang, *Chem. Commun.*, 2012, **48**, 10422-10424.
8. S. Q. Zhang, F. L. Jiang, Y. Bu, M. Y. Wu, J. Ma, X. C. Shan, K. C. Xiong and M. C. Hong, *CrystEngComm*, 2012, **14**, 6394-6396.
9. A. Schneemann, V. Bon, I. Schwedler, I. Senkovska, S. Kaskel and R. A. Fischer,

Chem. Soc. Rev., 2014, **43**, 6062-6096.
10. J. Heine and K. Muller-Buschbaum, *Chem. Soc. Rev*, 2013, **42**, 9232-9242.
11. M. Gustafsson, A. Bartoszewicz, B. n. Martín-Matute, J. L. Sun, J. Grins, T. Zhao, Z. Y. Li, G. S. Zhu and X. D. Zou, *Chem. Mater.*, 2010, **22**, 3316-3322.
12. C. Y. Sun, S. X. Liu, D. D. Liang, K. Z. Shao, Y. H. Ren and Z. M. Su, *J. Am. Chem. Soc.*, 2009, **131**, 1883-1888.
13. L. Cui, G. P. Yang, W. P. Wu, H. H. Miao, Q. Z. Shi and Y. Y. Wang, *Dalton Trans*, 2014, **43**, 5823-5830.
14. H. L. Wang, D. P. Zhang, D. F. Sun, Y. T. Chen, L. F. Zhang, L. J. Tian, J. Z. Jiang and Z. H. Ni, *Cryst. Growth Des.*, 2009, **9**, 5273-5282.
15. S. Q. Zhang, F. L. Jiang, M. Y. Wu, J. Ma, Y. Bu and M. C. Hong, *Cryst. Growth Des.*, 2012, **12**, 1452-1463.
16. L. Croitor, E. B. Coropceanu, A. E. Masunov, H. J. Rivera-Jacquez, A. V. Siminel and M. S. Fonari, *J. Phys. Chem. C*, 2014, **118**, 9217-9227.
17. B. Xu, J. Xie, H. M. Hu, X. L. Yang, F. X. Dong, M. L. Yang and G. L. Xue, *Cryst. Growth Des.*, 2014, **14**, 1629-1641.
18. Q. X. Liu, Q. Wei, X. J. Zhao, H. Wang, S. J. Li and X. G. Wang, *Dalton Trans*, 2013, **42**, 5902-5915.
19. X. Zhao, J. Dou, D. Sun, P. Cui and Q. Wu, *Dalton Trans*, 2012, **41**, 1928-1930.
20. Q. Zhu, C. Shen, C. Tan, T. Sheng, S. Hu and X. Wu, *Chem. Commun.*, 2012, **48**, 531-533.
21. J. Pan, F. L. Jiang, M. Y. Wu, L. Chen, Y. L. Gai, S. M. Bawaked, M. Mokhtar, S. A. Al-Thabaiti and M. C. Hong, *Cryst. Growth Des.*, 2014, **14**, 5011-5018.
22. J. Pan, C. P. Liu, F. L. Jiang, M. Y. Wu, L. Chen, J. J. Qian, K. Z. Su, X. Y. Wan and M. C. Hong, *CrystEngComm*, 2015, **17**, 1541-1548.
23. S. Z. Zhan, M. Li, S. W. Ng and D. Li, *Chem. Eur. J.*, 2013, **19**, 10217-10225.
24. L. L. Han, T. P. Hu, K. Mei, Z. M. Guo, C. Yin, Y. X. Wang, J. Zheng, X. P. Wang and D. Sun, *Dalton Trans*, 2015, **44**, 6052-6061.
25. Z. F. Wu, B. Tan, J. Y. Wang, C. F. Du, Z. H. Deng and X. Y. Huang, *Chem. Commun*, 2015, **51**, 157-160.

26. J. S. Guo, G. Xu, X. M. Jiang, M. J. Zhang, B. W. Liu and G. C. Guo, *Inorg. Chem*, 2014, **53**, 4278-4280.
27. M. S. Wang, S. P. Guo, Y. Li, L. Z. Cai, J. P. Zou, G. Xu, W. W. Zhou, F. K. Zheng and G. C. Guo, *J. Am. Chem. Soc.*, 2009, **131**, 13572-13573.
28. J. Zheng, Y. D. Yu, F. F. Liu, B. Y. Liu, G. Wei and X. C. Huang, *Chem. Commun.*, 2014, **50**, 9000-9002.
29. T. H. Yang, R. A. S. Ferreira, L. D. Carlos, J. Rocha and F. N. Shi, *RSC Adv*, 2014, **4**, 7818-7825.
30. C. B. Liu, R. A. Ferreira, F. A. Almeida Paz, A. Cadiau, L. D. Carlos, L. S. Fu, J. Rocha and F. N. Shi, *Chem. Commun*, 2012, **48**, 7964-7966.
31. S. M. Abtab, A. Audhya, N. Kundu, S. K. Samanta, P. S. Sardar, R. J. Butcher, S. Ghosh and M. Chaudhury, *Dalton Trans*, 2013, **42**, 1848-1861.
32. B. Bhattacharya, R. Dey, P. Pachfule, R. Banerjee and D. Ghoshal, *Cryst. Growth Des.*, 2013, **13**, 731-739.
33. Y. Wu, G. P. Yang, Y. Zhao, W. P. Wu, B. Liu and Y. Y. Wang, *Dalton Trans*, 2015, **44**, 3271-3277.
34. J. Guo, D. Sun, L. L. Zhang, Q. Yang, X. L. Zhao and D. F. Sun, *Cryst. Growth Des.*, 2012, **12**, 5649-5654.
35. E. L. Eliel and S. H. Wilen, *Stereochemistry of Organic Compounds*, Wiley: New York, 1994; Chapter 1913.
36. J. Liu, H. B. Zhang, Y. X. Tan, F. Wang, Y. Kang and J. Zhang, *Inorg. Chem*, 2014, **53**, 1500-1506.
37. C. A. Bauer, T. V. Timofeeva, T. B. Settersten, B. D. Patterson, V. H. Liu, B. A. Simmons and M. D. Allendorf, *J. Am. Chem. Soc.*, 2007, **129**, 7136-7144.
38. Y. Q. Huang, B. Ding, H. B. Song, B. Zhao, P. Ren, P. Cheng, H. G. Wang, D. Z. Liao and S. P. Yan, *Chem. Commun*, 2006, 4906-4908.
39. D. Thirion, M. Romain, J. Rault-Berthelot and C. Poriel, *J. Mater. Chem*, 2012, **22**, 7149-7157.
40. R. Q. Fan, Y. L. Yang, Y. B. Yin, W. L. J. Hasi and Y. Mu, *Inorg. Chem*, 2009, **48**, 6034-6043.

41. Y. Cui, Y. Yue, G. Qian and B. Chen, *Chem. Rev.*, 2012, **112**, 1126-1162.
42. Y. Cui, R. Song, J. Yu, M. Liu, Z. Wang, C. Wu, Y. Yang, B. Chen and G. Qian, *Adv. Mater.*, 2015, **27**, 1420-1425.
43. E. J. McLaurin, L. R. Bradshaw and D. R. Gamelin, *Chem. Mater.*, 2013, **25**, 1283-1292.
44. A. E. Albers, E. M. Chan, P. M. McBride, C. M. Ajo-Franklin, B. E. Cohen and B. A. Helms, *J. Am. Chem. Soc.*, 2012, **134**, 9565-9568.
45. A. Cadiau, C. D. S. Brites, P. M. F. J. Costa, R. A. S. Ferreira and L. D. Carlos, *ACS Nano*, 2013, **7**, 7213-7218.
46. A. H. Shelton, I. V. Sazanovich, J. A. Weinstein and M. D. Ward, *Chem. Commun*, 2012, **48**, 2749-2751.
47. Y. L. Gai, F. L. Jiang, L. Chen, Y. Bu, M. Y. Wu, K. Zhou, J. Pan and M. C. Hong, *Dalton Trans*, 2013, **42**, 9954-9965.
48. I. Jess, P. Taborsky, J. Pospisil and C. Nather, *Dalton Trans*, 2007, 2263-2270.
49. D. Sun, M. Z. Xu, S. S. Liu, S. Yuan, H. F. Lu, S. Y. Feng and D. F. Sun, *Dalton Trans*, 2013, **42**, 12324-12333.
50. S. Yuan, Y. K. Deng and D. Sun, *Chem. Eur. J.*, 2014, **20**, 10093-10098.
51. S. Gao, R. Q. Fan, X. M. Wang, L. S. Qiang, L. G. Wei, P. Wang, H. J. Zhang, Y. L. Yang and Y. L. Wang, *J. Mater. Chem. A*, 2015, **3**, 6053-6063.
52. R. R. Hu, C. F. A. Gómez-Durán, J. W. Y. Lam, J. L. Belmonte-Vázquez, C. M. Deng, S. J. Chen, R. Q. Ye, E. Peña-Cabrera, Y. C. Zhong, K. S. Wong and B. Z. Tang, *Chem. Commun*, 2012, **48**, 10099-10101.
53. Z. H. Yan, L. L. Han, Y. Q. Zhao, X. Y. Li, X. P. Wang, L. Wang and D. Sun, *CrystEngComm*, 2014, **16**, 8747-8755.
54. G. M. Sheldrick, *SHELXL 97 Program for Crystal Structure Refinement*, University of Göttingen, Germany, 1997.
55. G. M. Sheldrick, *SHELXL 97 Program for Crystal Structure Solution*, University of Göttingen, Germany, 1997.